IRSN

INSTITUT
DE RADIOPROTECTION
ET DE SÛRETÉ NUCLÉAIRE

Faire avancer la sûreté nucléaire

The Napa Earthquake, California (M=6; 24/08/2014)

Post-seismic survey report, with special focus on surface faulting

RT/PRP-DGE/2015-00018

Pôle radioprotection, environnement, déchets et crise

Service de caractérisation des sites et des aléas naturels

INQUA
Founded 1928

IRSN
INSTITUT
DE RADIOPROTECTION
ET DE SÛRETÉ NUCLÉAIRE

Pôle radioprotection, environnement, déchets et crise

Service de caractérisation des sites et des aléas naturels

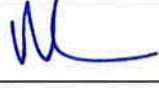|	
Demandeur	D3P12
Référence de la demande	Affaire 30001295/0070
Numéro de la fiche programme	—
Processus de rattachement	R4

THE NAPA EARTHQUAKE, CALIFORNIA (M=6; 24/08/2014)

Post-seismic survey report, with special focus on surface faulting

Stéphane Baize, Oona Scotti

Bureau Risques Sismiques pour la Sûreté des Installations

Rapport PRP-DGE n° 2015-00018

	Réservé à l'unité		Visas pour diffusion		
	Auteur(s)	Vérificateur	Chef du **SCAN**	Directeur DGE	Directeur Général Adjoint *
Noms	S. BAIZE, O. SCOTTI	S. HOK	V. REBOUR	F. BESNUS D. GAY	J. JOLY
Dates	18.01.2016	18.01.2016	18|01|16	18.01.2016	
Signatures					

DIFFUSION : Libre ☒   Interne ☐   Limitée ☐

*si nécessaire

LISTE DE DIFFUSION

Nom	Organisme
Giovanni Bruna	IRSN/DG
Nathalie Lemaître	IRSN/DSDP
Emmanuel Raimond	IRSN/PSN-RES/SAG
Jean-Philippe Tardivel	IRSN/PSN-EXP/SES/BEGC
François Besnus	IRSN/PRP-DGE/EC
Didier Gay	IRSN/PRP-DGE/EC
Vincent Rebour	IRSN/PRP-DGE/SCAN/EC
Laurent Guimier	IRSN/PRP-DGE/SCAN/EC
BERSSIN - Tous	IRSN/PRP-DGE/SCAN/BERSSIN
Ioannis Papanikolaou	INQUA/TERPRO / Agricultural University of Athens, Greece
Christoph Gruetzner	INQUA/TERPRO / Dpt Earth Sciences, University Cambridge, U.K.
Petra Stepančikova	INQUA/TERPRO / Institute Rock Structure and Mechanics, Prague, Czech Republic

RESUME

Le séisme de Napa en Californie (Mw=6, profondeur 10 km) s'est produit le 24 août 2014, provoquant d'importants dégâts à cause du mouvement sismique et de la rupture de surface. Dans la ville de Napa, le mouvement fort a atteint 0,4 g, affectant préférentiellement les bâtiments construits avant le Building Code, et la répartition des dommages a été en partie contrôlée par la géométrie 2D du bassin de Napa. Ce séisme remet en question les relations empiriques utilisées dans les études d'aléa sismique pour relier magnitude et paramètres de rupture de surface, avec un déplacement maximum mesuré de 45 cm et une longueur de rupture de 12,5 km, valeurs élevées pour une magnitude modérée. Certaines sections de la faille principale ont glissé de façon asismique, tandis que des ruptures secondaires ont été observées à plus de 2 km de la faille principale. La communauté scientifique a utilisé un large panel de techniques, de la cartographie classique aux imageries modernes (InSAR, LiDAR), offrant un retour d'expérience riche pour l'étude des séismes futurs et la mise à jour des bases de données sismotectoniques (e.g. ruptures de surface). Enfin, outre ces spécificités sismotectoniques, il sera intéressant de suivre les conséquences de ce séisme en termes de réglementation et de prévention.

ABSTRACT

The Napa earthquake (Mw=6; depth 10 km) occurred on the August 24th, 2014 and caused severe damages because of both ground motion and surface displacement. Large strong motion was recorded in the Napa City area (0.4 g), preferentially affecting the pre-Building Code facilities, and damage pattern was also controlled by the 2D geometry of the Napa Basin. This event questions the scaling relationships usually applied in seismic hazard studies to infer magnitude from measurable surface faulting parameters, with high values of maximum displacement (45 cm) and surface rupture length (12.5 km) for such a moderate magnitude. Huge amount of afterslip took place on several sections of the main strand, whereas secondary ruptures occurred more than 2 km off the main segment. The scientific community used a large panel of techniques, from classical field mapping to modern techniques (InSAR, LiDAR), providing an interesting feedback for the study of future earthquakes and the updating of seismotectonic databases (e.g. surface ruptures). Finally, besides these seismotectonic peculiarities of the quake, the regulatory and prevention aftermath will be followed carefully.

Content

1 _PRÉAMBULE_

Ce rapport a été écrit suite à notre visite de terrain destinée à étudier la rupture de surface associée au séisme de Napa (magnitude 6) en Californie, en décembre 2014, quelques mois après le séisme (24 août 2014).

Ce document a été écrit en anglais pour être transmis à nos collègues de l'INQUA avec lesquels nous travaillons à l'élaboration d'une base de données mondiale des ruptures de surface. Cette étude de cas est particulièrement intéressante car elle traite d'un séisme 1) de magnitude modérée, gamme de magnitude très peu représentée dans les bases de données actuelles, 2) présentant plusieurs ruptures secondaires d'amplitude significative, à des distances relativement importantes de la rupture principale (quelques kilomètres). Ce cas est également intéressant à analyser car il tombe dans la gamme des séismes possibles dans le contexte français et plus généralement européen intraplaque.

2 INTRODUCTION

The scope of this report is connected to a self-funded research program of IRSN which includes a section dedicated to surface ruptures associated with moderate size earthquakes.

The M6 Napa earthquake occurred on August 24th, 2014 at 3:20 AM (local time), along the West Napa Fault System (WNFS) (Figure 1). This earthquake is of primary interest for the INQUA-TERPRO community, in preparation of the 2015-2019 proposals focused on the constitution of a worldwide database of surface ruptures and on the updating/upgrading of magnitude-surface faulting relationships, especially for the moderate magnitude events. We anticipate that the ISSC-EBP Phase 2 project of IAEA will largely benefit from the gathered knowledge on this earthquake.

The Napa earthquake surface rupture is the first one to affect Northern California since the San Andreas earthquake (M7.8, April 18, 1906) and the second in the state to have damaged a populated area after the San Fernando earthquake (M6.6, February 9, 1971) in Southern California. Surface fault displacement occurred along a 12-km-long main strand, as well as along shorter secondary strands. The effects of the event were and will be therefore intensively studied to get a relevant feedback for earthquake preparedness and resilience.

Due to its moderate magnitude, this event can also be considered as an interesting analogue for understanding the seismotectonic processes and their relationship with surface effects and for evaluating the relevant methodologies, which both could concern a typical crustal earthquake in intraplate areas elsewhere in the world (including in Europe). The Napa earthquake evidences that moderate magnitude earthquake can produce extensive surface slip, both on primary and remote secondary strands. It also underlines the relevance of modern techniques to map and measure surface deformation, especially in the low-moderate magnitude range.

This report is based on our own field observations in Napa area in December 2014 (2 days) and on the already significant references dealing with this event. The most significant ones are the following:

- The EERI report (2014) which emphasizes the shaking effects on buildings, lifelines, infrastructures, focusing on engineering aspects;
- The GEER report (Bray et al., 2014), developing the engineering and geotechnical points (including the effects of surface faulting);

- The USGS Open-file 2014-1249, also referred as Hudnut et al. (2014), which analyzes the shaking and faulting effects of the earthquake, as well as the key recovery factors and a forecast of afterslip hazard in Browns Valley district of Napa;
- A special issue of Seismological Research Letters (Volume 86, Number 2A March/April 2015) with two particular papers which give an overview on the earthquake and its effects (Brocher et al., 2015) and provide key points on the location of damages (Boatwright et al., 2015).

The report first describes the seismotectonic and geological background of the earthquake and the West Napa Fault (section 2), then presents the seismological aspects of the event in two parts: starting with the earthquake source characteristics (section 3), followed by the strong motions and their effects on the structures (section 4). In a 5th section, the report focuses on the surface faulting and its effects.

3 SEISMOTECTONIC AND GEOLOGICAL BACKGROUND OF THE WEST NAPA FAULT SYSTEM

The 2014 Napa earthquake occurred north of the San Pablo Bay, at the South end of the Napa Valley in the greater San Francisco Bay (Figure 1). The region belongs to the California Coast Range province and is characterized by northwest trending valleys and low mountain ranges. The earthquake occurred on the West Napa Fault System (WNFS) which is a NNW-striking right-lateral fault zone between two major active fault systems, the Hayward-Rodgers Creek Fault system to the West and the Concord-Green Valley Fault system to the East. These fault systems are part of the 80-km-wide set of major faults that forms the boundary between the Pacific and North American plates. Through this plate boundary, almost 4 cm/yr of right lateral displacement are accommodated.

The WNFS was, prior to the event, recognized in the USGS Quaternary Fault Database as a Pleistocene fault, active between 15,000 and 130,000 years (Figure 1). No evidence was clearly known about its Holocene activity, with the exception of the "airport" portion. Accordingly, only this latter segment was considered as an Earthquake Fault in the Alquist-Priolo Act of California, which means that investigation are then required to reduce the threat to public health and safety posed by the fault. However, the WNFS is included in the UCERF3 (Uniform California Earthquake Rupture Forecast, version 3), which is a forecast of earthquake probabilities based on fault models (Field et al., 2013); in this study, a best-estimate slip rate of 1 mm/yr is assigned to the WNFS, mainly on the basis of geomorphic expression.

Historically, the North San Pablo Bay area was severely shaken and damaged during the Hayward Fault Earthquake in 1868 (M=6.8), the 1906 San Andreas Fault earthquake (M=7.8), and particularly during the 1898 Mare Island earthquake (M=6.3). The most significant damages during this quake were reported along the northern shoreline of the San Pablo Bay, 10 to 15 km south of the Napa earthquake epicenter. The source fault of the 1898 event is still debated, but may be the Rodgers Creek Fault (RCF), another low-slip rate fault of the area (Hough, 2014). The 2000 Yountville earthquake (Mw=4.9) occurred closed to the WNFS trace, north of Napa where it caused slight damages.

The Napa Valley is underlain by marine Cretaceous and Jurassic sedimentary rock which are covered by Early Tertiary sedimentary rocks and Late Tertiary volcanic rocks. The valley itself is composed of a thick pile of loose sediments (Napa Valley Basin, 2,000 m thick in Napa) lying above the bedrock (Secondary and Tertiary rocks). This sedimentary pile ends with up to 160 m of Pleistocene alluvial deposits and with 10 m of recent Holocene alluvial

deposits (sands, gravels, silts and clays). Figure 1 presents the 2014 rupture traces (labels from Hudnut et al., 2014) against the surficial geology. The 'A' segment is the longest (>12 km) where the largest displacement has been observed (46 cm). Segments 'B' to 'F' are secondary segments accommodating distributed deformation.
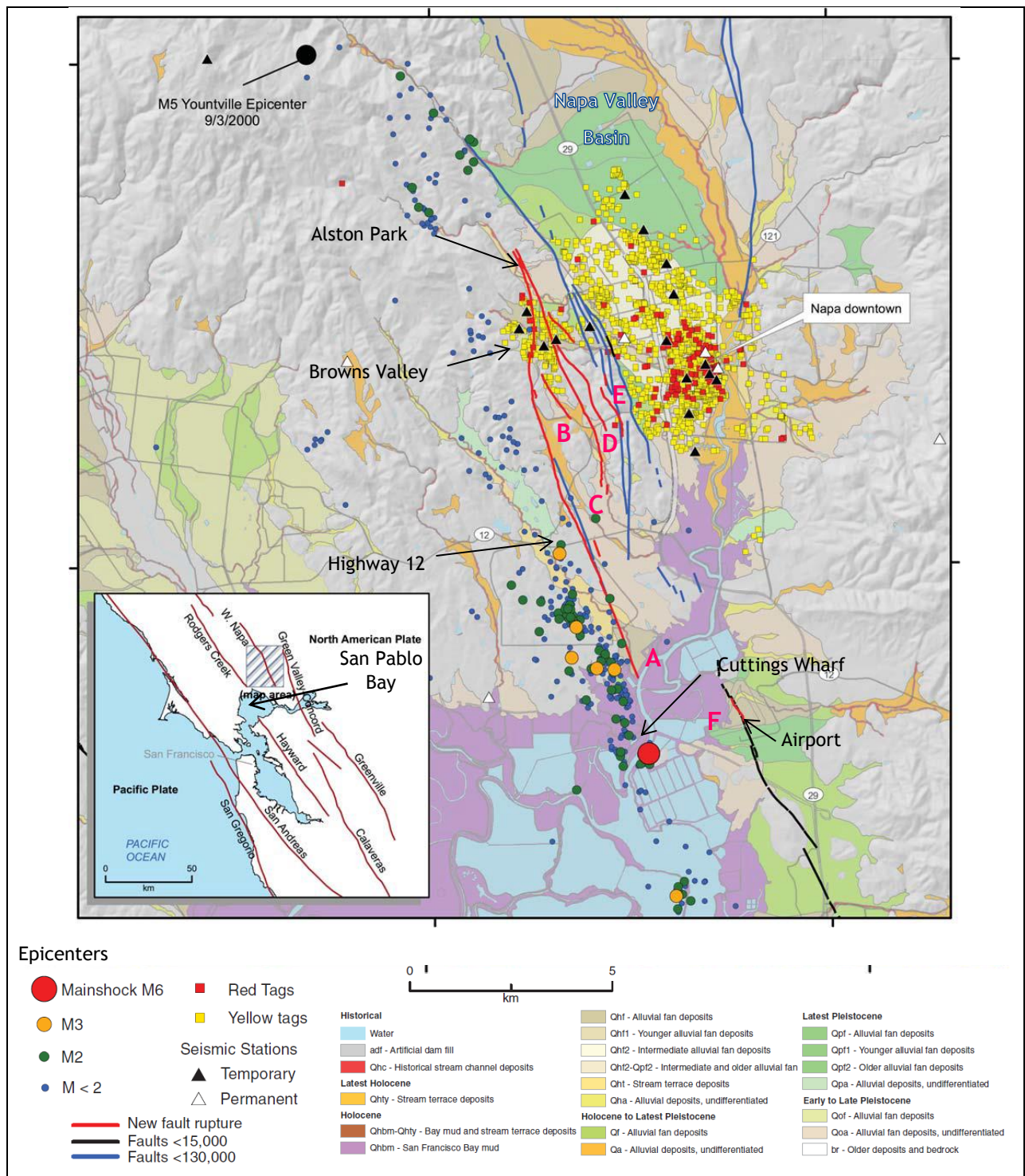
Figure 1 : Synthetic map with the 2014 surface rupture in red (letter labels of 2014 ruptures are those in Hudnut et al., 2014), and previously mapped faults (Holocene in black; Pleistocene in blue), with locations of red- and yellow-tagged buildings (from Boatwright et al., 2015), as well as locations of permanent (unfilled triangles) and temporary (filled triangles) seismic stations. The inset map shows the location of the major faults in the San Francisco Bay area. Figure modified from Brocher et al. (2015).

4 SOURCE CHARACTERISTICS OF THE 2014 NAPA EARTHQUAKE

The focal mechanism attests to a pure dextral strike-slip faulting along a N165°E plane dipping to the SW. The USGS provides the following parameters for the main shock hypocenter location:

Latitude	Longitude	Depth (km)
38.216°N	122.312°W	11

Preliminary slip models were published by the USGS few hours after the quake, then updated with new processing. Based on the inversion of GPS or seismological data, they show that the rupture was initiated at depth in the south and then propagated to the north and up-dip to the surface. Maximum values of slip at depth come close to 1 meter (Figure 2). The fault slip history model suggests explanations for the damages observed in Napa city and its suburbs:

- first, the main slip zone is located right below the city, which can be an explanation to the largest deformation in this area, close to the fault;
- second, the focal mechanism being a pure right lateral strike-slip, the city area lies in an extensional quadrant of the deformation, which is likely to promote secondary fault breaks;
- finally, the up-dip and northward rupture propagation focused radiated wave energy toward the city and possibly increased damages there.

Later fault slip model based on joint inversion of seismic waveform, GPS and InSAR data gave similar amounts and pattern of slip (Dreger et al., 2015).

The relocation of aftershocks highlighted two main fault planes, which intersect at depth where the mainshock and a majority of aftershocks nucleate. The "main" fault plane strikes N160°E and dips 70° to the southwest; its projection to the surface approximately coincides with the surface rupture trace (Figure 1). The area between the main fault and Napa city where numerous secondary segments are mapped matches with the shallow part of the large slip patch location. The "secondary" fault plane strikes N-S and gently dips (35°) to the east, with no surface expression known.
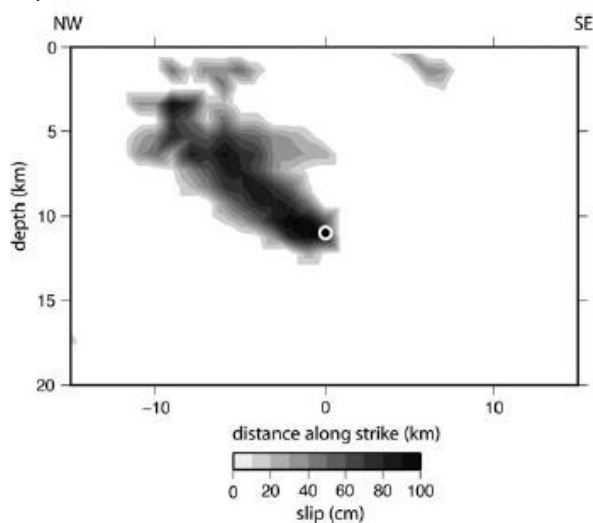

Figure 2: Slip model for the M6 earthquake, obtained from inversion of seismic data (white circle : hypocenter). From Brocher et al. (2015)

5 STRONG MOTIONS AND EFFECTS ON BUILDINGS

Large strong motion values were recorded in the Napa area, provoking damages to many buildings. According to Kishida et al. in Bray et al. (2014), a mean PGA of 0.4 g occurred in Napa Downtown at an approximate distance of 4 km from the fault surface, with a maximum value of 0.61 g recorded on the north-south component of the Main St Napa station (Boatwright et al, 2015). The highest value (PGA=0.7 g) was however measured to the south, at Carquiñez Bridge, probably due to a combination of path and site effects or soil-structure interaction (Kishida et al. in Bray et al., 2014).
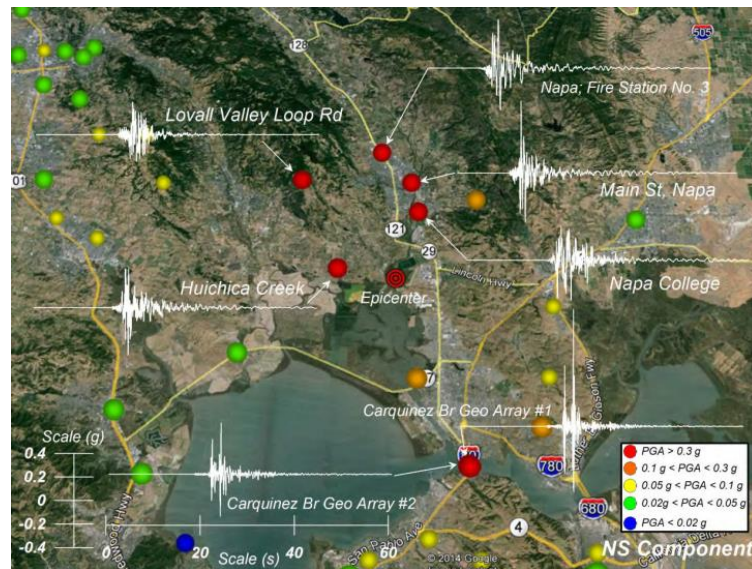

Figure 3: Acceleration time series, N-S component, recorded at stations where PGA higher than 0.3 g. Stations from CGS, USGS, NCSN networks (Kishida et al., 2014)

After the main shock, four instruments were set up in the Napa city to record aftershocks and estimate the site effects with spectral ratios. The relative amplification between these 4 stations is low between 1 and 20 Hz, suggesting that the ground motion associated with the 2014 main shock was quite homogenous across Napa downtown (Hudnut et al, 2014).

The available records of near-field and remote stations (distances ranging between 3 and 300 km) were compared with several Ground Motion Prediction Equations usually used in the western USA (e.g. NGA West, Abrahamson et al., 2008) and it appears that the measured motion decreases with distance more rapidly than predicted, indicating that regional attenuation is stronger in the Napa region than elsewhere in California (on which the GMPEs were built) (Brocher et al., 2014). At near distances, predictions and observations match much better. Records also highlight the northerly rupture directivity with positive residuals (records > prediction) along the Napa and Sonoma valleys to the north. As noted by Brocher et al. (2015), the Napa earthquake recordings will provide a significant strong motion dataset in the near-field, which will be of major interest for engineering purposes.

The event was responsible for significant damages mostly focused in Napa, 10 km north of the epicenter. Damages extend from Browns Valley to the west to Napa Downtown, where some residential buildings suffered shifting on their foundations, failure of walls or collapse of chimneys. In the historic part of Napa, masonry buildings were also severely damaged (Figure 4). Building inspectors examined hundreds of buildings which were ranked as

severely (red tags) or moderately (yellow tags) damaged[1]. There is a significant correlation between the age of buildings and the damages in Napa downtown (Boatwright et al., 2015). When tagged structures are plotted against the 1951 city map of Napa, there is a clear relation with the developed zones in that time. This shows that the damages due to the earthquake preferentially affected the old buildings, and that the lack of significant damages around may result from the efficiency of the Building Code of 1975. A second factor controlled the extension of damages, explaining the tagged distribution outside Napa downtown. Hudnut et al. (2014) and Boatwright et al. (2015) note that there is a reasonable correlation between the damage pattern and the location of the basin edges –especially in the west and the east (Figure 5). According to them, this suggests a "2D amplification" at the basin scale, due to these dipping impedance interfaces. The same authors underline that there is a poor correlation between surface geology and distribution of damages.

With the advent of the DYFI (Did You Feel It?) system, there is no longer a systematic program to assess intensity distributions of USA earthquakes from either conventional surveys or field investigations (Susan Hough, written communication). The current practice in the USA is to assign intensities based on the geocoded DYFI online records. Hough (2014) notes "*that traditional intensity distributions imply more dramatic damage patterns than are documented by more spatially rich DYFI data*" and "*that traditionally assigned intensity values tend to be inflated by a fundamental bias towards reporting of dramatic rather than representative effects*". According to Boatwright et al. (2015), the average value obtained in Napa center is around 8 with DYFI data, with individual values higher than 8.5 (Figure 6). These intensity values correspond to severe shaking and moderate/heavy damages[2] in the MMI scale. In the Browns Valley (Napa suburbs close to the northern end of the fault), the MMI intensity based on DYFI reports also reaches the degree 8 (Figure 6). Individual description of damages provided by EERI (2014) in Napa center are consistent with MMI intensity 9, with buildings shifted on their foundations or unbraced cripple walls.

To get a large spatial representation of MMI intensity, the USGS automatically publishes an "instrumental intensity map" (ShakeMap) which is processed from ground motion recordings and other information such as surface geology, in order to help in crisis and aftermath management. The "instrumental intensity" is calibrated according to a regression of peak acceleration and velocity amplitudes versus DYFI intensity for eight significant California earthquakes (source USGS website). The strong shaking recorded in the valley, with a local peak instrumental intensities of 9 at Napa Fire Station (EERI, 2014) and of 8.5 recorded at the Main St Napa station (named N106) (see Figure 3 for locations), comes out with a large area predicted at intensity 8 (Boatwright et al., 2015).

Finally, to conclude, seismological records in Napa Downtown are globally consistent with the observed damages and reported DYFI intensities. The maximum intensity based on witness reports, ground motion and damages is 8, with local estimation reaching 8.5. The Napa city damages were increased with 2D site effects due to the basin geometry. In addition, records highlight the northerly rupture directivity which contributed, probably, to the relative high level of damages.

---

[1] A red tag means that the building has been severely damaged and it is no longer safe and the entrance has to be avoided; a yellow tag means that the building has been moderately damaged. Use of the building is limited.
[2] Damage is slight in specially designed structures; considerable damage in ordinary substantial buildings with partial collapse. Damage is great in poorly built structures. Fall of chimneys, factory stacks, columns, monuments, walls. Heavy furniture are overturned (source: USGS website)

Figure 4: Damages to a masonry building in the historical Napa center (Brown St-2nd St)
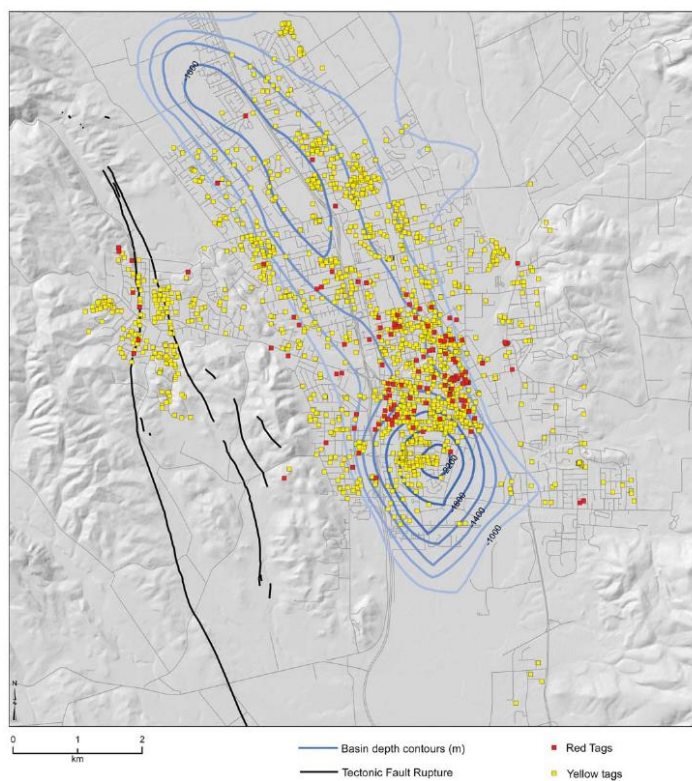

Figure 5 : Red and yellow tags plotted over contours of the depth to basement inferred from the Bouguer gravity anomaly (from Boatwright et al., 2015)
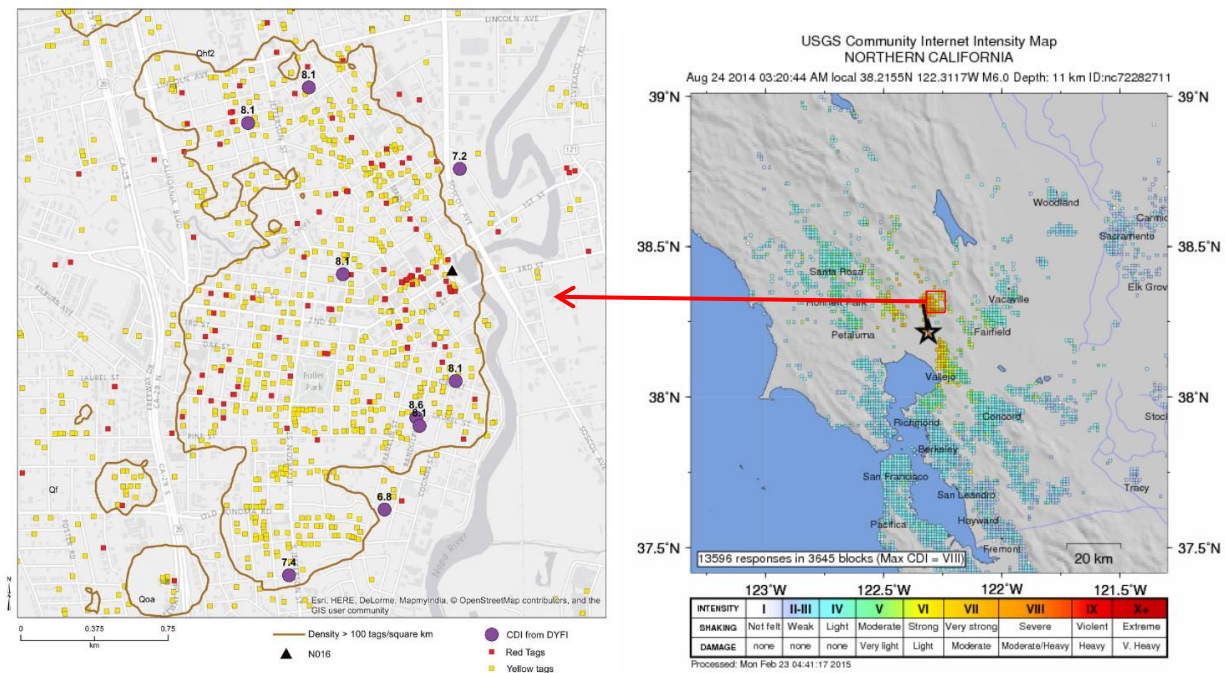
Figure 6 : Left: Comparison of red- and yellow-tagged building locations and DYFI intensities (MMI) (from Boatwright et al., 2015). Right: regional DYFI intensity map based on geocoded reports (source USGS); epicentral intensity is estimated to 8. Black star and line represent the epicenter and the fault trace, respectively.

6 ENVIRONMENTAL EFFECTS

The major environmental effect of the M6 Napa earthquake was surface faulting. Very few secondary effects like landslides, ground failures and liquefaction were triggered, in spite of the presence of several sand boils mapped in Napa along the river channel. The scarcity of liquefaction may be due to two main reasons (Brocher et al., 2015). On one hand, the region experienced before the earthquake an exceptional period of drought resulting in a low elevation water table (for instance, observed at 13 m depth in the Napa Valley), precluding potential liquefaction to reach the surface. On the other hand, the superficial deposits of the Napa valley are too fine grained to be prone to liquefaction (Brocher et al., 2015).

Emergent springs and increased flows in streams were reported after the event (Rytuba and Holzer, 2014). These flows were documented in previously dry creeks in the hills surrounding Napa at distances of 19 km to the west, 6 km to the east, and 18 km to the north of Napa. This covers an approximate surface area of 450 km², which underwent intensities higher than 6 according to USGS DYFI intensity map. Data from a gaging station suggest that the increased flow appeared coevally or very soon after the quake.

6.1 SURFACE RUPTURE

Surface rupture was mapped in the few hours after the quake. Geologists from various Californian universities, institutes or companies (UC Davis, Berkeley, CGS, USGS, Fugro, etc) started their field reconnaissance early in the morning, observing and measuring the ground displacements. The area was also covered by aerial overflights, and early InSAR processing allowed tracking lineaments and then checking fault displacements.

Figure 7 presents the interferogram generated using Sentinel-1A images acquired on 7/8/2014 and 31/8/2014, respectively before and after the 24/8/2014 mainshock. The two rounded lobes around the Napa River show the

large-scale ground deformation during the earthquake, which have induced phase changes in radar signal appearing as the rainbow-colored shapes. These lobes are typical of strike-slip earthquake signature on interferometry images. Each fringe corresponds to a ground displacement of 28 mm toward or away from the satellite. The fault is visible as two short strands marked by white arrows, where fringes are disrupted: the eastern one crosses the Napa airport where 1 cm right-lateral offset has been measured on the field; the western strand coincides with the southernmost part of the main rupture trace in the Cuttings Wharf area, where total slip is estimated around 30-35 cm. The northern section of the main rupture strand is obscured (no fringes shown) because no correlation could be found between the pre- and post-radar datasets (Figure 7).

Figure 8 presents the interferogram generated using UAVSAR (Uninhabited Aerial Vehicle Synthetic Aperture Radar) images acquired on 29/5/2014 and 29/8/2014 by the NASA's Jet Propulsion Laboratory. That picture shows that the surface rupture was complex and occurred on multiple strands. We add on Figure 8 our interpretation of strand locations (letter labels as of Hudnut et al., 2014). The initial picture gives a preliminary estimation of surface displacement amount, which has been updated since and generally lowered: actually right lateral displacement is less than 40 cm around the Highway 12 (Fremont Drive), instead of 80 cm as indicated on the picture. Each fringe represents here a ground displacement of 12 centimeters towards or away from the satellite.
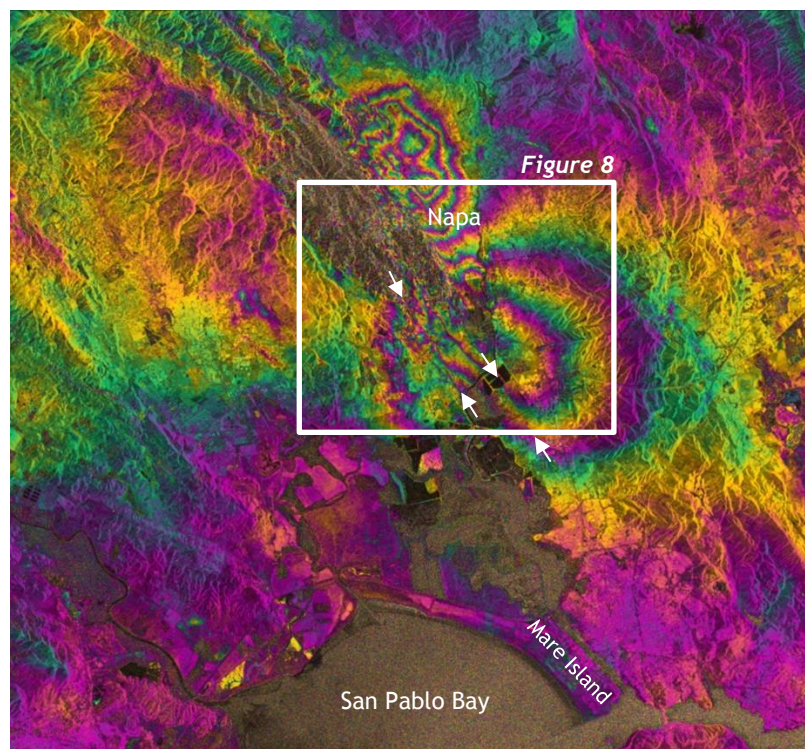

Figure 7: InSAR interferogram calculated with Sentinel-1 radar data. Source ESA/COMET, available at http://www.esa.int/. White arrows indicate the location of surface faults that can be inferred from this dataset.

We compiled the field observed offset data provided by different groups available on the Clearinghouse website (http://www.eqclearinghouse.org/2014-08-24-south-napa/), including the values provided by Hudnut et al. (2014), and also including our own measurements made on 2014, December 12th and 13th (Figure 9). The fault trace is constituted of dextral fractures (Figure 10) often appearing as left-stepping fractures (Figure 11). The local conditions, with dry fields and abundance of vine rows, as well as the profusion of paved roads, greatly facilitated the observation of surface deformation (see Figure 12 and Figure 13). Measured offset values are reported in Table 1.
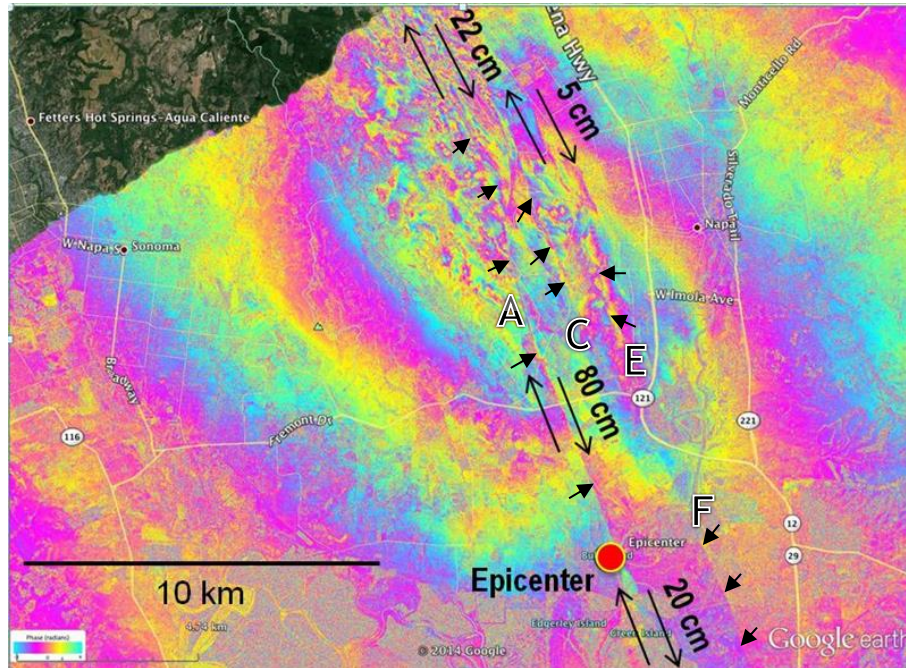
Figure 8 : InSAR interferogram calculated with UAVSAR data. Source: JPL. Preliminary indications of slip values are in black (significantly lowered after field survey). Black arrows with letter labels show the fault traces. Letter labels are those of Hudnut et al. (2014)

In December 2014, 4 months after the quake, most of the deformation features could still be observed, except for the features on paved roads because most had been removed by road works. Surface faulting occurred along several fault strands between the Alston Park in Napa and the Cuttings Wharf (Figure 1). The westernmost trace (A) is the longest (12.5 km) and the maximum offset was measured on it (≈50 cm), approximately 10 km north of the epicenter. In its northern part, it is coincident with a previously mapped "bedrock" fault that juxtaposes Mesozoic rocks with Tertiary layers, which was however not recognized as active. Around the Highway 12 (NAPA 23), it is superimposed on a fault trace that is reported to have been active before 15 ky but after 130 ky in the USGS database. Note that a post-2014 earthquake trench, dug close to Los Carneros Avenue (NAPA19, Figure 9) across the 2014 surface rupture, revealed that this fault trace has effectively been active previously during the Quaternary (Gordon Seitz, pers. comm. during AGU 2014).

The trace C is the other large rupture that appeared during the earthquake, with offsets up to 8 cm. The fault was previously unknown there. Traces B and D are short and do not coincide with previously mapped faults. The trace E is partly coincident with a bedrock fault between sandstones and volcanics of the Miocene. Another post-2014 earthquake trench revealed that the E strand has been active during the Quaternary and probably caused past earthquakes with surface ruptures (Hudnut et al., 2014). Trace F at the Napa County Airport, with small 2014 fault displacement (1 cm), coincides with a previously mapped trace of the West Napa Fault Zone, which was ranked in the Alquist-Priolo Fault Database as an Earthquake Fault (i.e. Holocene fault).
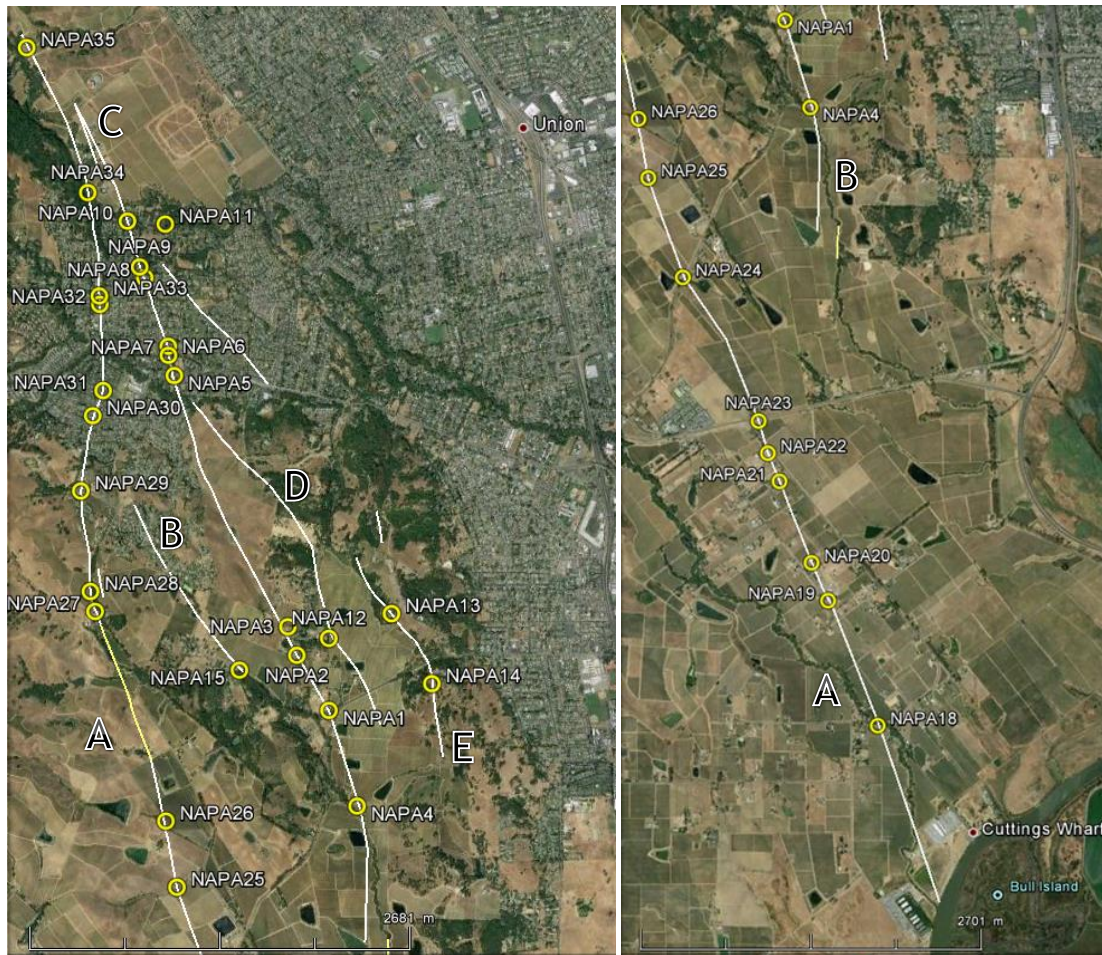
Figure 9 : Database of field slip measurements plotted on the USGS earthquake fault traces (base map: Google Earth image).

Figure 10: Examples of linear features as markers of right-lateral offset along the main strand (A), as we could observe them in December 2014, 4 months after the quake. Left: a fence is offset of 35 cm south of highway 12 (NAPA 22); yellow arrows underline the fault trace; white arrows the relative displacement. Right: Dextral offset of vine rows south of Browns Valley (NAPA 28).

Point	Segment (see Figure 1)	Net Slip (cm)	Distance from Southern tip of the segment (USGS trace) (m)	Perpendicular Distance To Mainfault (segment A) (m)	Surficial Geology	Source
NAPA1	C	8.7	1673	1290	Alluvium*	GEER
NAPA2	C	5.7	2121	1210		GEER/FUGRO
NAPA3	C	4.8	2332	1220		Fugro
NAPA4	C	1.0	966	1345		USGS
NAPA5	C	5.0	4280	499		Morelan-Trexler/Brooks
NAPA6	C	7.0	4493	462		IRSN
NAPA7	C	2.0	4429	459		Morelan-Trexler
NAPA8	C	4.0	5004	321	Contact Paleogene sediments and Alluvium	Morelan-Trexler
NAPA9	C	8.0	5088	287		USGS
NAPA10	C	3.0	5423	225	Alluvium	USGS
NAPA11	X	1.0		488		Morelan-Trexler
NAPA12	D	5.0		1469	Paleogene Sediments	USGS
NAPA13	E	3.0		1965	Neogene Volcanic rocks	USGS
NAPA14	E	6.0		2064	Paleogene Sediments	USGS
NAPA15	B	1.0		785	Alluvium	USGS
NAPA16	X	1.0		2897		USGS
NAPA17	X	1.5		2390		Morelan-Trexler
NAPA18	A	28.0	1479	0		USGS
NAPA19	A	33.0	2540	0		USGS/Baize-Scotti
NAPA20	A	24.0	2866	0	Contact Pliocene Sediments / Alluvium	Baize-Scotti
NAPA21	A	34.0	3555	0		USGS
NAPA22	A	32.1	3794	0		Baize-Scotti/Dawson
NAPA23	A	30.0	4056	0		Baize-Scotti
NAPA24	A	30.0	5328	0	Contact Cretaceous sediments / alluvium	Baize-Scotti
NAPA25	A	27.0	6147	0		USGS
NAPA26	A	45.0	6619	0	Alluvium	USGS
NAPA27	A	46.0	8177	0	Contact Cretaceous/Paleogene sediments	USGS/Dawson
NAPA28	A	40.3	8321	0		USGS/Dawson
NAPA29	A	37.0	9029	0		Baize-Scotti
NAPA30	A	15	9562	0	Alluvium	Morelan-Trexler
NAPA31	A	12	9754	0		USGS
NAPA32	A	6	10362	0	Contact Paleogene sediments and Alluvium	Morelan-Trexler
NAPA33	A	11	10420	0		USGS
NAPA34	A	1	11154	0	Paleogene sediments	USGS
NAPA35	A	5	12234	0		USGS

*Alluvium refers to Holocene to Pleistocene alluvial sediments

Table 1 : Synthesis of displacement values associated with the Napa earthquake (used in Figure 14 andFigure 15).

NAPA22; Cuttings Wharf Road, 200 m south of highway 12

Dec 2014

Figure 11: Two views of the same fault outcrop at NAPA22 waypoint (offset 32 cm), illustrating the left-stepping fractures.

Figure 12: Right-lateral displacement (28 cm) of the Las Amigas road, on the southern section of the 'A' strand, cumulates on several parallel segments (NAPA18). At this place, afterslip is high (more than 90% of the net slip). Picture december 2014.

In order to feed a database, we analyze the surface fault rupture evidence distribution along and off the main fault strand (A segment). The fault traces were digitized on Google Earth from the figure 19 of Hudnut et al. (2014), and then transferred to ArcGIS. We superimposed these traces on the USGS LIDAR image (Hazards Data Distribution System Explorer), to check their reliability and adjust the location of displacement evidence to the real fault trace, if needed.

Our data compilation is graphically reported in Figure 14 for the main strand A (main strand). Along this trace, the offset values are reported along the **12.5 km-surface rupture length,** starting from the southern tip. Along this A trace, the **maximum displacement** was measured between Leaning Oak and Henry Road at **46 cm** (i.e. between NAPA 26 and NAPA 29), 8 km north of the southern tip and almost 10 km north of the epicenter. Lienkaemper et al. (2014) and Brocher et al. (2015) state that the 2014 slip at this point was essentially coseismic, respectively 45 cm (data updated in November 2014) and 46 cm (paper published in February 2015).

The **average displacement** value from our dataset is **25 cm** along the A segment.

It is important to remind that this compilation deals with the total slip, summing up the coseismic slip and afterslip after several months. This aseismic deformation mainly occurred during the few hours and days after the shock, only along the A trace (main strand), and was unevenly distributed along the A fault trace (see 6.2).

For the distributed faulting evidences, we report the slip values with respect to their shortest distance to the main fault trace (A). Centimetrics to decimetric values are reported as far as 2-3 km from the main trace (A) (Figure 15). We could observe some remaining evidences of distributed faulting along the C strand, like a 7 cm-displaced curb in the Browns Valley area (Covey Ct, NAPA6) or a vertically and horizontally offset fence (Congress Valley Rd, NAPA1) (Figure 16).

As mentioned by different authors (Hudnut et al., 2014; Brocher et al., 2015), not only the earthquake caused an unusual amount of surface displacement (Maximum Displacement MD=46 cm; Average Displacement AD=25 cm) over an unusual Surface Rupture Length (SRL=12.5 km) for such a moderate magnitude, but also it produced a significant amount of distributed displacement (max. 8 cm) at large distances to the main trace (2.5-3 km). Actually, as shown on Figure 15, the distributed displacement pattern resembles the one of an M=6.5 earthquake like the Borrego earthquake in Southern California (1968).

In the Browns Valley area, we could observe ground deformations that were not directly associated with surface faulting. Compressional and extensional features, which were revealed by man-made equipment like road pavements and sidewalks, are concentrated over a wide zone west of the surface rupture (segment A). Typical compressional features are buckled sidewalks and extensional are open fractures (Figure 17).

These features were mapped and measured by Bray et al. (2014), who consider them as proofs of tectonic strain. By measuring the pre- and post-lengths, they could determine a weak shortening of about 0.01-0.02% all over the area, both in N-S and E-W direction.

Figure 13: Some outstanding evidences of fault rupture associated with the Napa earthquake as they can be observed on the LIDAR (source: USGS) along the A trace. A: In the northern section, one can observe the left-stepping fractures (yellow arrows) and the dextral offset of the path (red arrow); B: In the middle section, the fault rupture cuts the vine rows where we could measure a 30 cm dextral displacement of a fence (NAPA24 waypoint); C: Along southern section of the rupture, south of Highway 12, the rupture coincides with a gentle scarp facing to the east (underlined by hillshading).
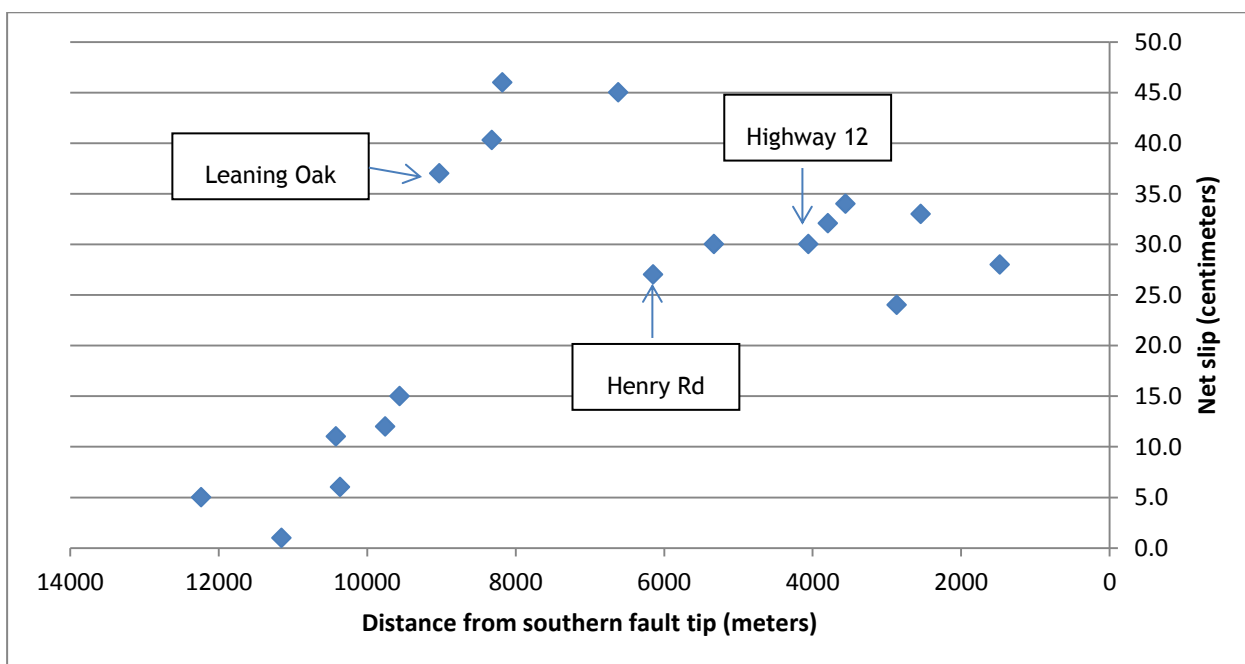

Figure 14 : Distribution of surface slip along the main fault trace, aggregating data from various sources and integrating displacement over several months.
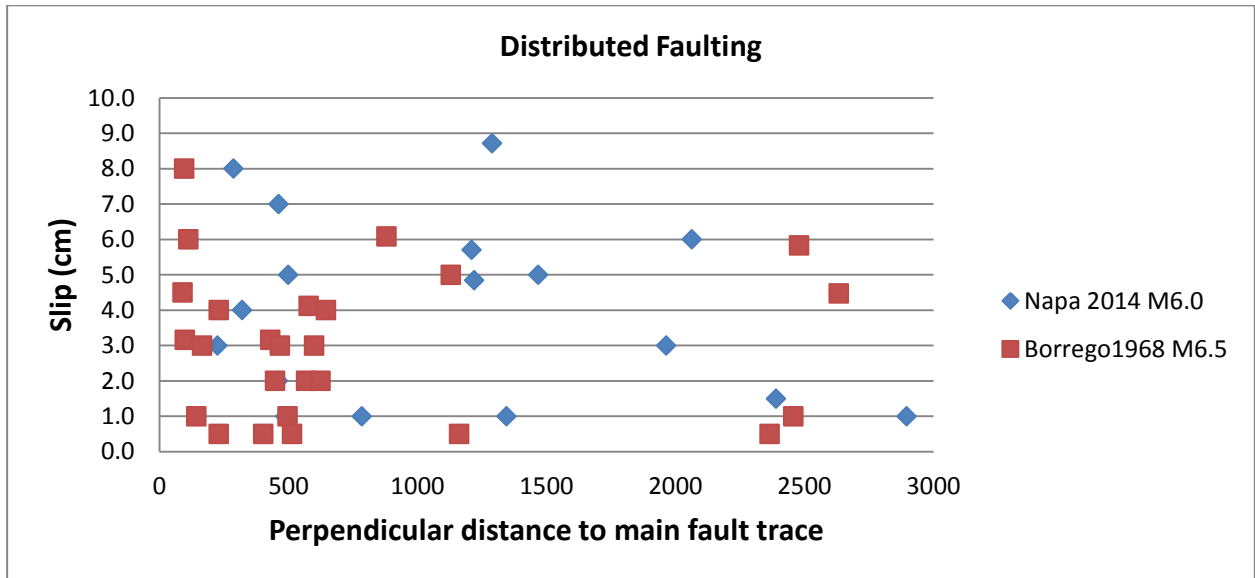
Figure 15 : Distributed slip values compiled from various sources for the Napa earthquake. Values for the M6.5 Borrego Mountain earthquake (Petersen et al. 2011) are also plotted for comparison.

Figure 16: Some evidences of distributed faulting as they could be observed in December 2014 along the C segment. Left: to the north, offset curb in Covey Ct in Browns Valley inhabited area (NAPA6). Right: to the south, displaced fence in Congress Valley Road (NAPA1) (Figure 9).

Buckled sidewalk

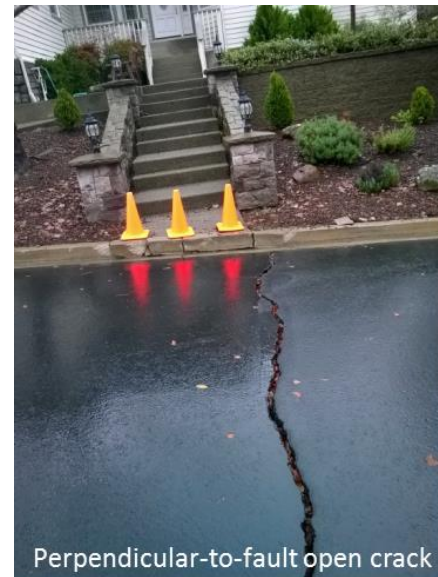Perpendicular-to-fault open crack

Figure 17: Ground deformation in the vicinity of the fault trace, Browns Valley area (GEER, 2014). Tension evidences include open cracks; compression evidences buckled sidewalks.

6.2 AFTERSLIP

Besides the unusual length and displacement amount, the Napa earthquake is "exceptional" because of the large amount of afterslip that characterizes some sections of the main trace (A). Afterslip is the continuation of slip along a fault rupture after the quake. Generally, this afterslip is faster following the main shock, and it regularly decreases with time.

In Napa, the afterslip is clearly highlighted by the UAVSAR interferogram picture presented in Figure 18. The change in color, from purple to green along a north-south line is obviously due to post-seismic faulting (location NLOD). No similar change is visible around the secondary strands and particularly around the C strand (location NELW). Field evidences of afterslip are numerous, as shown on Figure 19, mainly in the southern portion of the fault (between Highway 12 and Cuttings Wharf) but also in the northern one (Leaning Oak).

As the fault crosses a populated area, the USGS decided to monitor the fault which experienced postseismic displacement in order to measure the time series and the final goal is to propose a forecast for the long-term afterslip. A network of 6 alignment arrays, 5 of them located across the primary strand, was installed immediately after the quake. Two of these arrays are mapped in Figure 18 (NLOD and NELW) in the populated area (Browns Valley). Given the relative short term dataset (90 days), the data were extrapolated with an appropriate time-dependent function. This model has been developed and calibrated with data from monitored Californian earthquakes (AFTER model) and it predicts an exponential decay of displacement with time and predicts that deformation ceases after a certain time. Modelling the Napa earthquake indicates that the total slip south of the maximum slip location (km 10 on the horizontal scale on Figure 20; NAPA27-28 area) is dominantly postseismic (50-100%), whereas to the north it is dominantly coseismic (50-100%) (Figure 20) (Lienkaemper et al., 2014).

As suspected from successive field observations through time, the alignment array measurements confirm that afterslip was very large in the first hours and days and then steadily slowed down (Figure 20). Fifty percent of the afterslip occurred after 1 day, 75% after 5 days and most of the afterslip was done after 60 days. The AFTER model forecasts that in the long-term afterslip can however last for years. Thus, in the populated Browns Valley area, the

main strand between Leaning Oak and Patrick Road (more or less the one in the imprint of Figure 18) may experience 5 to 15 cm of afterslip in the next 3 years.
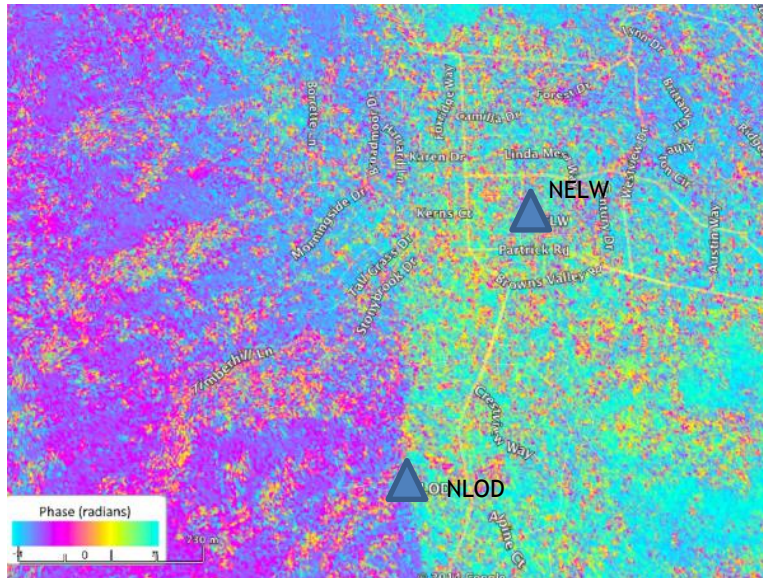

Figure 18: JPL UAVSAR interferogram processed with 2 images shot on the 29/8, five days after the mainshock, and on the 22/10/2014 (Hudnut et al., 2014). Triangles show the positions of monitoring arrays installed by USGS after the earthquake. NLOD: Leaning Oak alignment array (close to NAPA29) and NELW: Ellen Way alignment array (close to NAPA6).

Figure 19: Field evidences of afterslip along the main trace. Top: Leaning Oak (NAPA29), northern section of main segment (left picture from UC Davis); Middle: Highway 12 (picture from Bray et al., 2014, GEER report), southern section of the main segment (NAPA23); bottom: Los Carneros avenue, southernmost part of this segment (NAPA19); blue and yellow lines were drawn on the fault rupture in the first hours after the mainshock and their later offset illustrates the postseismic slip (afterslip).
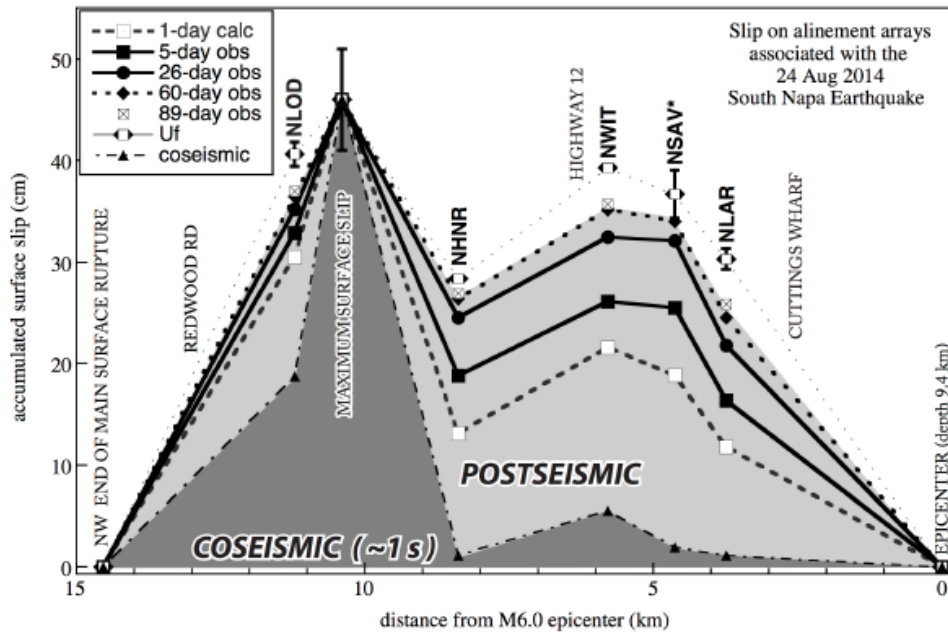
Figure 20: Evolution in space and time of afterslip at the earth surface (from Lienkaemper et al., 2014, in Hudnut et al., 2014). Epicenter (south) is at right; Browns Valley (north) is at left, between 11 and 13 km. Coseismic slip amount could not be measured, thus is estimated from seismological data. Afterslip is then reported according to alignment array data and it increases with time (between 5 and 89 days). Uf is the forecast total final displacement.

6.3 EFFECTS OF SURFACE FAULTING ON INFRASTRUCTURES

The Geotechnical Extreme Events Reconnaissance (GEER) Association did an extensive survey of the damages due to faulting in the Browns Valley area, a residential neighborhood west of Napa (Bray et al., 2014).

The Browns Valley area, in which facilities are dominantly single-family residences consisting of single-story wood-frame structures, was extensively affected by surface faulting. The GEER field teams examined ≈40 structures in 3 days and, although the houses were damaged during shaking, the engineers could discriminate the effects of faulting. They could observe new open cracks going through the structures or concrete slabs, horizontal or vertical displacements of walls or foundations (e.g. Figure 21), offsets of curbs, displacements of structures away from the adjacent ground or from their foundations, etc. In some houses with pier-and-grade beam foundations, relative displacement due to faulting provoked torsion and cracking of walls. In December 2014, we could still observe damages and restoration works in progress, like red-tagged houses located on the main fault that necessitate complete reworking of their foundations (Figure 22): the technique is to "uplift" the house, in order to keep its integrity, and repair the foundation damage. In the neighborhood of the illustrated case, around 10-15 cm surface displacement was measured. In December 2014, we could even observe a house with damaged foundation on the secondary segment C, where offset was around 5 cm (Figure 23).

Besides residences, surface faulting damaged above all road asphalt. Traffic was temporarily disrupted but rapidly reopened as roads were fixed. Few underground utilities and other infrastructure where the fault traversed developed areas (Browns Valley) were affected, but in a limited extension. For instance, we infer that a PG&E underground utility could have been affected by surface faulting in Covey Ct (NAPA6) where we could measure a 7 cm sidewalk offset (Figure 16). At the Stone Bridge School in the Carneros District (NAPA19), surface rupture cracks developed in the asphalt parking and in the adjacent yard to the north, and there cuts a large-diameter PG&E gas pipeline. The GEER team (Bray et al., 2014) was informed on little or no deformation of the pipeline and their own observation could not confirm any offset of the utility.

Figure 21 : Example of a strip footing foundation displaced by faulting (picture from Bray et al., 2014)

Figure 22 : Work in progress on a residence foundation affected by faulting, located on the primary fault trace A (close to NAPA30 waypoint, White Cliff Circle). The house has been uplifted for the repairing. Surface slip was measured to be around 10-15 cm.

Figure 23 : Work in progress on a residence foundation affected by faulting, located on the secondary (distributed) fault trace C (close to NAPA2 waypoint). The wall has been destroyed by workers after the earthquake. A 5-6 cm Surface slip was measured on the close road pavement just after the earthquake.

6.4 DISCUSSION

6.4.1 ENVIRONMENTAL INTENSITY

The Napa earthquake led to an (almost) unique environmental effect, which is surface faulting. According to the Environmental Seismic Intensity Scale (Reicherter et al., 2009), a 12.5 km long surface trace together with displacements up to 40 cm would be associated with an epicentral ESI intensity of 9, even 10. The lateral extension of hydrological effects mentioned after the Napa earthquake (spreading over 400 km^2) is consistent with ESI intensity 9 (Table 2).

In the MMI scale, which deals with effects on structures, the intensity degree '9' corresponds to "*Violent shaking*" and "*Damage considerable in specially designed structures; well-designed frame structures thrown out of plumb. Damage [is] great in substantial buildings, with partial collapse. Buildings shifted off foundations*", and the level '10' to "*Extreme shaking*" and damages such as follows: "*Some well-built wooden structures destroyed; most masonry and frame structures destroyed with foundations. Rails bent.*" These shaking effects have not been extensively reported in the various consulted reports either close (Browns Valley area) or far (Napa Center) from the fault, with the exception of several residences which shifted on their foundations because of shaking. In the Browns Valley area, the residences, in a great majority designed against damage, generally resisted quite well to seismic motion, whereas downtown old buildings are not designed and suffered shaking. A general agreement thus is that epicentral intensity approaches 8.

The apparent discrepancy between "environmental" and "structural" estimations may have a simple explanation. The environmental estimation is inflated by the fact that a large part of measured slip has not been responsible for shaking because appeared during the postseismic phase. Actually, Lienkaemper et al. (2014) estimated that the contribution of coseismic surface slip to the total event surface slip, integrated along the whole fault trace, is only of 27%.

I_0	PRIMARY EFFECTS		SECONDARY EFFECTS
	SURFACE RUPTURE LENGTH	MAX SURFACE DISPLACEMENT / DEFORMATION	TOTAL AREA
IV	-	-	-
V	-	-	-
VI		-	-
VII	(*)	(*)	10 km^2
VIII	Several hundreds meters	Centimetric	100 km^2
IX	1- 10 km	5 - 40 cm	1000 km^2
X	10 - 60 km	40 - 300 cm	5000 km^2
XI	60 – 150 km	300 –700 cm	10000 km^2
XII	> 150 km	> 700 cm	> 50000 km^2

(*) Limited surface fault ruptures, tens to hundreds meters long with centimetric offset may occur essentially associated to very shallow earthquakes in volcanic areas.

Table 2: Synthetic table matching intensity levels (ESI scale) with measured environmental effects (based on Reicherter et al. 2009). Primary effects concern the surface faulting parameters; secondary effects concern induced phenomena by shaking or far-field deformation (liquefaction, landsliding, hydrological effects, etc).

6.4.2 EMPIRICAL RELATIONSHIPS BETWEEN MAGNITUDE AND FAULT PARAMETERS

When compared to regional (California) data of similar magnitude historical events (since 1948), the 2014 earthquake is largely above the mean values for maximum displacement (MD) and surface rupture length (SRL) which are 6.5 cm and 5 km respectively (Brocher et al., 2015). Also, when compared to a worldwide dataset of strike-slip earthquakes that can be represented by the relevant Wells and Coppersmith (1994) regressions, the Napa earthquake falls outside the mean and standard deviation values (Figure 24).
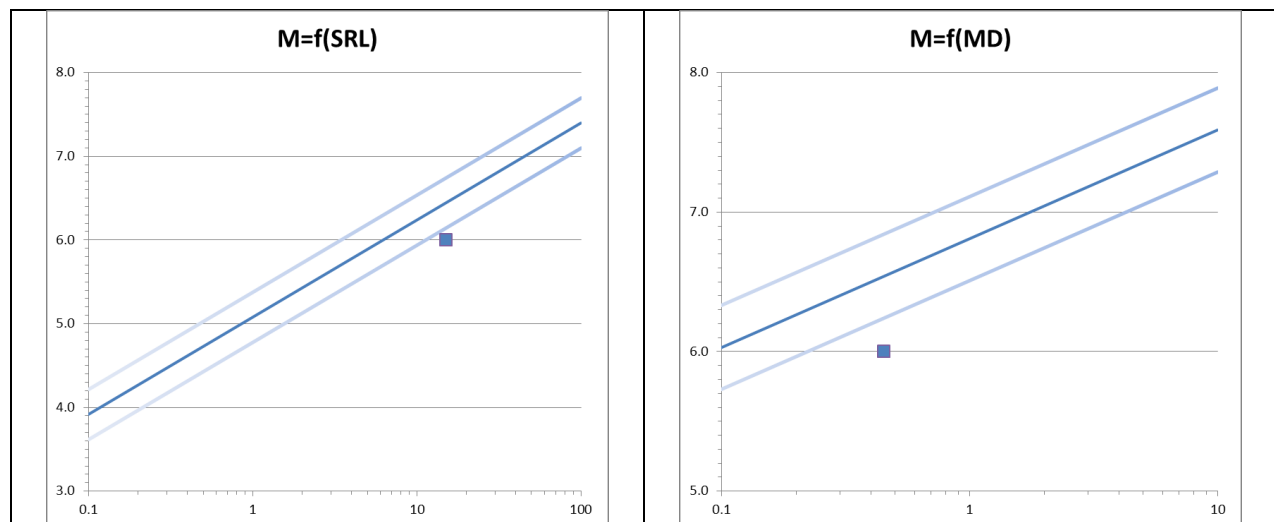

Figure 24: Napa Earthquake values of Surface Rupture Length (SRL, left) and Maximum Displacement (MD, right) plotted against a 'Wells and Coppersmith' mean correlation with magnitude, including standard deviation.

In siting studies, a fault is often analyzed through paleoseismological investigations which provide slip rates, displacement values per event, and sometimes surface rupture length. The Wells and Coppersmith (1994)'s empirical relationships are usually used to predict the magnitude associated with possible future events from fault parameters. As many other earthquake cases, this earthquake questions the relevance of the Wells and Coppersmith (1994)'s relationships (e.g. Baize et al., 2015). Actually, these "scaling laws" were built with incomplete datasets of historical events, especially concerning large events with significant surface expression. However, scientific community has now access to faint deformation features thanks to the modern techniques like InSAR, LiDAR, etc. and we can now think about upgrading the earthquake rupture database with moderate magnitude events, or other categories of earthquakes which are under-represented in existing databases (reverse earthquakes, strong but blind events, etc.).

More recent empirical relationships are proposed in literature, but often they rely on a similar dataset of historic and recent earthquakes, and like Wells and Coppersmith (1994), explore limited parameters to propose regression relations between magnitude and fault parameters (e.g. fault kinematics and geodynamic context in Leonard, 2010). Many modern case studies demonstrate that surface rupture length or coseismic surface displacement depend on the depth of the earthquake, shape of the fault plane with respect to ground surface, shear modulus, and many other factors like stress drop. If we can build an extensive fault database in the future, the inclusion of these kinds of parameters is likely to improve the regression relations between magnitude and fault parameters. We might be inspired by how the Ground Motion Prediction Equations were developed by researchers who assembled a large and standardized database of strong motion records that different groups could tap into for

proposing their own regression equations considering key parameters. These parameters might range from surface geology, focal depth, structural context, etc; most of them being accessible.

The Napa earthquake also revealed that a large amount of afterslip can occur, even for moderate magnitude crustal events. In paleoseismic studies, this possibility is generally not taken into consideration and displacement is directly converted to magnitude, assuming that the whole offset occurred during the earthquake. Because we should not be able to distinguish between coseismic slip and afterslip in stratigraphic records of a trench, the magnitude might sometimes be over-estimated.

6.4.3 COMPARISON OF THE SECONDARY FAULTING MEASUREMENTS WITH AVAILABLE DISPLACEMENT-TO-FAULT DISTANCE REGRESSION

In their paper published in the Bulletin of the Seismological Society of America, Petersen et al. (2011) provide a regression function which gives the expected "off-fault" displacement "d" that could occur at distance "r" from the main fault trace on a secondary strand, during an earthquake of magnitude "M" on the primary fault.

$$Ln\ (d) = 1.4016 \times M - 0.1671 \times ln\ (r) - 6.7991\ (\pm\ 1.1193)$$

This regression has been calibrated with a limited dataset of seven strike-slip earthquakes that occurred in California, greater than magnitude 6.5. This regression is extrapolated in recent studies for nuclear power plant safety down to magnitudes 5.0 and 6.0, respectively for Krško NPP in Slovenia (Rizzo, 2013) and for Diablo Canyon NPP in California (NRC, 2012). Taking into account the values measured after the Napa earthquake on secondary segments, we think that the Petersen regression and its uncertainties could be updated. Indeed, some measured displacements of the Napa dataset fall out of the expected uncertainty range, with a higher mean value (Figure 25).
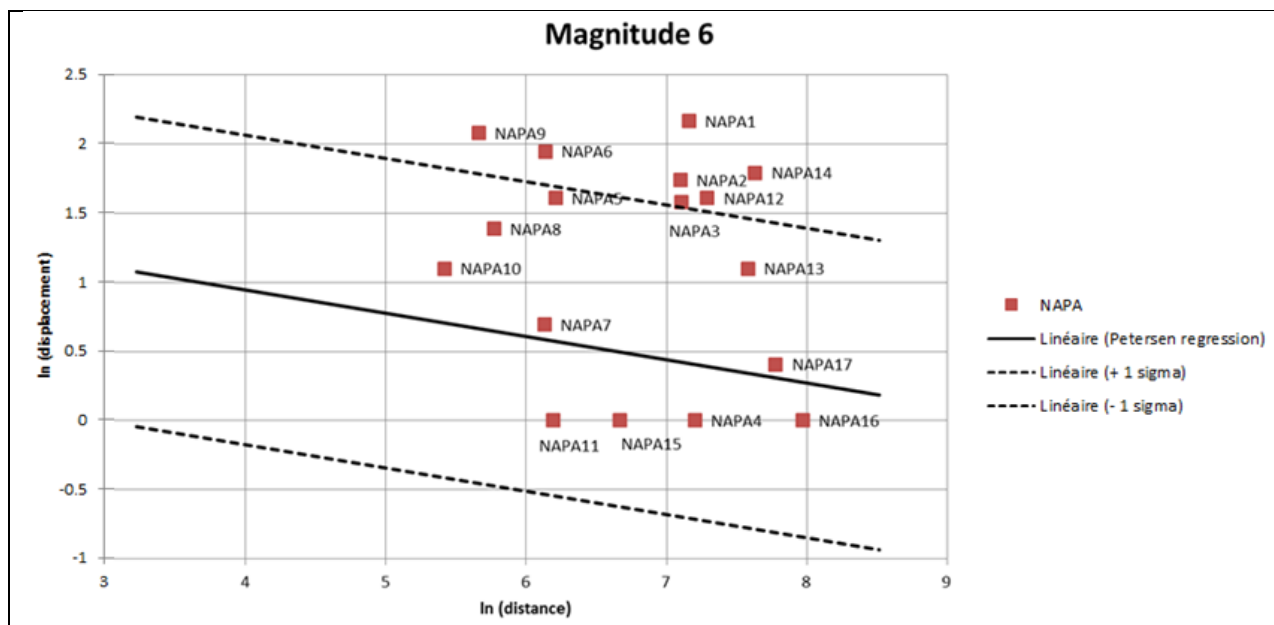

Figure 25: Graph illustrating the Napa secondary ruptures measurements with respect to the predictive regression of an M= 6 event (Petersen et al., 2011). For location of measurement points, refer to Figure 9.

7 <u>CONCLUSION</u>

As a conclusion, we emphasize the following points. From an engineering seismological point of view, the 2014 Napa M6 earthquake gave new data in the near-field which will help in constraining near-field GMPEs. Seismological aspects have not been emphasized in this report and we focused on its geological effects. Despite strong ground motions and the presence of a large alluvial plain which was extensively surveyed after the earthquake, no liquefaction or other secondary environmental effects were triggered. Accordingly, we can anticipate that similar M6 events in the past, in a similar environment with analogue climatic/hydrologic components, would have left no (or very few) trace of secondary effect in the geological records. In a seismic hazard assessment perspective, the Napa earthquake case confirms that the exclusive use of the secondary environmental recordings is delicate to achieve the "completeness" of the paleoseismic catalogue: this example clearly emphasizes that "no evidence of paleoearthquake from secondary effect analysis" does not mean "no earthquake". A deep knowledge of local geomorphic/climatic background during the last 10/100 kyr is required, and we have to account for parameters like liquefaction index or water table depth. However, paleoseismological trench results on the major segment -where paleoearthquakes are recognized- show that this approach is appropriate to infer the WNF activity in the Napa case.

The occurrence of large coseismic displacements, together with a large surface rupture length, leads to question the extensive use of the common scaling relationships between magnitude and geologically-measured fault parameters (maximum displacement, surface rupture length) such as published by Wells and Coppersmith (1994). With the observed maximum displacement and surface rupture length, their application would lead to an M=6.5 event, dramatically higher than the "true" magnitude. Certainly, a reassessment of these existing relationships should be done, including new parameters such as crustal properties, soil conditions, etc. Furthermore, the Napa case shows that the Petersen regression (2011), used to predict the off-fault displacement that could occur on secondary fault strands during an earthquake, must also be re-evaluated. This relation has been calibrated on a limited dataset of Californian earthquakes (M≥6.5) but is extrapolated to lower magnitudes in safety studies. The measured displacements in several places after the 2014 Napa earthquake fall clearly out the predicted uncertainty range, with dramatically higher values.

In the light of the Napa earthquake case, a challenge is to factor out aseismic slip. Indeed, a significant part of slip (as inferred from the surface measurement) did not contribute to generating seismic motion. This can mean that, in geological records, the use of average surface displacement can introduce a bias and future challenges include anticipating an aseismic behavior on a fault.

In a perspective view, we emphasize that similar geodetic (including InSAR, alignment arrays) and geologic (field survey, LiDAR,…) investigations should be performed after future crustal earthquakes, to come out with additional enriched data on surface faulting. The general aim of is to increase the surface rupture dataset, coupled with an (re)assessment or updating of previous events, in order to eventually improve the attenuation relationships of surface displacement to distance. These relations are crucial to perform Probabilistic Fault Displacement Hazard Analysis (PFDHA), recommended for facility siting.

8 REFERENCES

Baize, S., McCalpin, J., Scotti, O., Costa, C., Cinti, F. R., Michetti, A. M., Okumura, K. , Dawson, T. (2015). Earthquake geology of shallow crustal faults and Seismic Hazard Assessment: Challenges ahead. Abstracts Volume 6th International INQUA Meeting on Paleoseismology, Active Tectonics and Archaeoseismology, 19-24 April 2015, Pescina, Italy, pp 37-40.

Boatwright, J., Blair, J. L., Aagaard, B. T., Wallis K. (2015). The Distribution of Red and Yellow Tags in the City of Napa. Seismological Research Letters, Volume 86, Number 2A, 361-368, doi: 10.1785/0220140234.

Bray, J., Cohen-Waeber, J., Dawson, T., Kishida, T., Sitar, N. (EDS) (2014). Geotechnical Engineering Reconnaissance of the August 24, 2014 M6 South Napa Earthquake. Report of the NSF Sponsored GEER Association Team, California Geological Survey, Pacific Earthquake Engineering Research Center, and U.S. Geological Survey, GEER Association Report No. GEER-037.

Brocher, T. M., Baltay, A. S., Hardebeck, J. L., Pollitz, F. F., Murray, J. R., Llenos A. L., Schwartz, D. P., Blair, J. L., Ponti, D. J., Lienkaemper, J. J., Langenheim, V. E., Dawson, T. E., Hudnut, K. W., Shelly, D. R., Dreger, D. S., Boatwright, J., Aagaard, B. T., Wald, D. J., Allen, R. M., Barnhart, W. D., Knudsen, K. L., Brooks, B. A., Scharer K. M. (2015). The Mw 6.0 24 August 2014 South Napa Earthquake. Seismological Research Letters, Volume 86, Number 2A, 309-326, doi: 10.1785/0220150004.

Dreger, D. S., Huang, M.-H., Rodgers, A., Taira, T., Wooddell., K. (2015). Kinematic Finite-Source Model for the 24 August 2014 South Napa, California, Earthquake from Joint Inversion of Seismic, GPS, and InSAR Data. Seismological Research Letters, Volume 86, Number 2A, 327-334, doi: 10.1785/0220140244.

EERI (2014). M 6.0 South Napa Earthquake of August 24, 2014. EERI Special Earthquake Report, 27 pages.

Field, E.H., Biasi, G.P., Bird, P., Dawson, T.E., Felzer, K.R., Jackson, D.D., Johnson, K.M., Jordan, T.H., Madden, C., Michael, A.J., Milner, K.R., Page, M.T., Parsons, T., Powers, P.M., Shaw, B.E., Thatcher, W.R., Weldon, R.J., II, and Zeng, Y. (2013). Uniform California earthquake rupture forecast, version 3 (UCERF3)—The time-independent model: U.S. Geological Survey Open-File Report 2013–1165, 97 p., California Geological Survey Special Report 228, and Southern California Earthquake Center Publication 1792, http://pubs.usgs.gov/of/2013/1165/.

Hough, S. (2014). Where was the 1898 Mare Island Earthquake? Insights from the 2014 South Napa Earthquake. AGU Fall Meeting, San Francisco, December 2014.

Hudnut, K.W., Brocher, T.M., Prentice, C.S., Boatwright, J., Brooks, B.A., Aagaard, B.T., Blair, J.L., Fletcher, J.B., Erdem, J.E., Wicks, C.W., Murray, J.R., Pollitz, F.F., Langbein, J., Svarc, J., Schwartz, D.P., Ponti, D.J., Hecker, S., DeLong, S., Rosa, C., Jones, B., Lamb, R., Rosinski, A., McCrink, T.P., Dawson, T.E., Seitz, G., Rubin, R.S., Glennie, C., Hauser, D., Ericksen, T., Mardock, D., Hoirup, D.F., and Bray, J.D. (2014). Key recovery factors for the August 24, 2014, South Napa earthquake: U.S. Geological Survey Open-File Report 2014–1249, 51 p., http://dx.doi.org/10.3133/ofr20141249.

Leonard, M. (2010). Earthquake Fault Scaling: Self-Consistent Relating of Rupture Length, Width, Average Displacement, and Moment Release. Bulletin of the Seismological Society of America, Vol. 100, No. 5A, pp. 1971–1988.

Lienkaemper, J.J., Brooks, B.A., DeLong, S.B., Domrose, C.J., and Rosa, C.M. (2014). Surface slip associated with the 2014 South Napa, California earthquake measured on alinement arrays. AGU Fall Meeting, San Francisco, December 2014.

NRC (2012). Confirmatory Analysis of Seismic Hazard at the Diablo Canyon Power Plant from the Shoreline Fault Zone.Research Information Letter 12-01. Available at http://a4nr.org/.

Petersen, M. D., T. E. Dawson, R. Chen, T. Cao, C. J. Wills, D. P. Schwartz, and A. D. Frankel (2011). Fault Displacement Hazard for Strike-Slip Faults. Bulletin of the Seismological Society of America, Vol. 101, No. 2, pp. 805–825, April 2011, doi: 10.1785/0120100035.

Reicherter, K., Michetti, A.M., Silva, P. G. (eds) (2009). Palaeoseismology: Historical and Prehistorical Records of Earthquake Ground Effects for Seismic Hazard Assessment. The Geological Society, London, Special Publications, 316, 1–10. DOI: 10.1144/SP316.1.

Rizzo Associates Inc. (2013). Probabilistic Fault Displacement Hazard Analysis – Krško East and West sites – Slovenia. Technical Report, available at http://www.ursjv.gov.si

Rytuba, J., Holzer, T. (2014). Sources of Increased Spring and Streamflow Caused by the 2014 South Napa Earthquake. AGU Fall Meeting, San Francisco, December 2014.

Wells, D. L., Coppersmith, K., J. (1994). New empirical relationships among magnitude, rupture length, rupture width, rupture area and surface displacement. Bulletin Seismo. Society America, 84, 974-1002.